Energy & Environmental Science

Cite this: *Energy Environ. Sci.*, 2011, **4**, 2316

www.rsc.org/ees

PAPER

Annealing treatment improves the morphology and performance of photovoltaic devices prepared from thieno[3,4-*c*]pyrrole-4,6-dione-based donor/acceptor conjugated polymers and CdSe nanostructures†

Chih-Yin Kuo,[a] Ming-Shin Su,[a] Guan-Yu Chen,[a] Ching-Shun Ku,[b] Hsin-Yi Lee[b] and Kung-Hwa Wei*[a]

Received 10th March 2011, Accepted 13th April 2011
DOI: 10.1039/c1ee01283e

We have prepared photovoltaic devices based on blend films of CdSe tetrapods and the donor/acceptor conjugated polymer PDTTTPD, which comprises 2,5-di(thiophen-2-yl)thieno[3,2-*b*]thiophene and thieno[3,4-*c*]pyrrole-4,6-dione units. The AM1.5 power conversion efficiency (PCE) of a photovoltaic device containing a PDTTTPD/CdSe tetrapod blend (1 : 9, w/w) that had experienced thermal annealing (130 °C, 20 min) was three times greater than that of the corresponding device incorporating the as-prepared PDTTTPD/CdSe tetrapod blend (2.9% *vs.* 1.0%). Synchrotron X-ray reflectivity revealed that annealing (*i.e.*, removal of pyridine ligands from the surfaces of the CdSe tetrapods) caused the thickness of the PDTTTPD/CdSe tetrapod blend film to decrease (and its average density to increase) relative to that of the as-prepared blend film. Transmission electron microscopy and atomic force microscopy revealed that thermal annealing enhanced the degree of aggregation of the CdSe tetrapods and induced denser morphologies, leading to substantially increased charge transport, which enhanced the PCE of the device.

Introduction

Solution-processing of bulk heterojunction (BHJ) photovoltaic devices, including those featuring polymer–polymer,[1–4] polymer–C_{60} derivatives,[5–10] and polymer–nanocrystal[11–17] blends, is an attractive area of investigation with many potential benefits—particularly for the rapid and economical preparation of flexible, large-area devices. The development of composite materials comprising a conjugated polymer as the hole acceptor and a solution-processable inorganic semiconductor nanocrystal as the electron acceptor for use in BHJ photovoltaic systems has recently undergone several major advances. For example, conjugated polymer/nanocrystal photovoltaic devices containing CdSe nanocrystals (one of the most investigated materials for use as the electron acceptor), fabricated in combination with poly-(3-hexylthiophene) (P3HT),[18–21] OC1C10 PPV,[22,23] MEH-PPV,[24] and the alternating polyfluorene copolymer APFO-3[25] as hole acceptors, have exhibited AM1.5G power conversion efficiencies (PCEs) in the range 1.4–2.6%. Moreover, large improvements in PCEs (up to 3.1%) have been obtained when combining CdSe tetrapods with poly[2,6-(4,4-bis-(2-ethylhexyl)-4*H*-cyclopenta [2,1-*b*;3,4-*b*′]-dithiophene)-*alt*-4,7-(2,1,3-benzothiadiazole)] (PCPDTBT).[26] The shape of the CdSe nanocrystals has a major effect on the device performance when blended with polymers.[27]

[a]*Department of Materials Science and Engineering, National Chiao Tung University, 1001 Ta Hsueh Road, Hsinchu, 30050, Taiwan, ROC. E-mail: khwei@mail.nctu.edu.tw; Fax: +886 35 724727; Tel: +886 35 731871*

[b]*National Synchrotron Radiation Research Center, 101 Hsin-Ann Road, Science-Based Industrial Park, Hsinchu, 30077, Taiwan, ROC*

† Electronic supplementary information (ESI) available: *J–V* characteristics and GIXRD patterns of the PDTTTPD/CdSe tetrapod photovoltaic devices. See DOI: 10.1039/c1ee01283e

Broader context

The solution processing of materials for use in thin film organic optoelectronic devices is an attractive area of investigation because of its easy and low-cost structure that reduces energy consumption during the fabrication of large-area devices. The morphology of the solution processed thin films is strongly affected by the processing parameters and subsequent thermal or solvent treatments. In particular, the photovoltaic performances of bulk heterojunction polymer solar cells that feature conjugated polymers as donors and semiconductor nanocrystals as acceptors critically depend on the nanoscale morphology in the active layers. The optimal phase domains in the active layer provide not only interfaces for the charge separation of photogenerated excitons but also percolation pathways for carrier transport to the respective electrodes, leading to improvement in devices' power conversion efficiency.

For example, the performance of devices incorporating tetrapod-shaped nanocrystals (tetrapods), which feature an optimal arrangement for electron extraction, is superior to that of devices incorporating nanorods or spherical nanocrystals.[22]

In principle, photovoltaic devices should exhibit excellent performance when incorporating polymer/CdSe nanocrystals in the BHJ because of the high absorption coefficient and tunable band gap of CdSe nanocrystals; their performance is, however, typically worse than that of polymer/fullerene BHJ photovoltaic devices because of the complicated surface structure of the nanocrystals.[28] The surfaces of inorganic semiconductor nanocrystals typically present long-chain, electrically insulating organic ligands, which must be shortened or removed for opto-electronic device applications.[29–32] A major challenge for research into inorganic semiconductor nanocrystals is the development of methods for ligand exchange or ligand removal, thereby decreasing the inter-nanocrystal spacing and creating denser and more-conductive films.

Conjugated polymers containing alternating donor (D) and acceptor (A) units in their main[33,34] or side[35,36] chains have been applied widely in BHJ photovoltaic devices because of their readily tunable electronic properties. The electron-deficient thieno[3,4-*c*]pyrrole-4,6-dione (TPD) moiety exhibits a symmetric, rigidly fused, coplanar structure with strong electron-withdrawing properties, making it a potentially useful system for increasing the strength and number of intramolecular/intermolecular interactions and lowering the highest occupied molecular orbital (HOMO) energy levels when incorporated into polymeric backbones, resulting in enhanced open-circuit voltages (V_{oc}) in BHJ solar cells.[37–40]

In this study, we investigated the effects of thermal annealing on the morphology and photovoltaic device performance of thin films incorporating the CdSe tetrapods and the D/A conjugated polymer PDTTTPD, comprising 2,5-di(thiophen-2-yl)thieno[3,2-*b*]thiophene and thieno[3,4-*c*]pyrrole-4,6-dione units. We expected the removal of pyridine ligands from the CdSe tetrapods' surfaces during the annealing process would affect the packing density and nanoscale morphology[41] of the active layer in the photovoltaic devices and, therefore, the device performance. The optimal arrangement of CdSe tetrapods in the active layer would provide not only interfaces for the charge separation of photogenerated excitons but also percolation pathways for carrier transport to the respective electrodes, thereby improving the devices' PCE. Here, we used attenuated total reflection Fourier transform infrared (ATR-FTIR) spectroscopy and a synchrotron X-ray reflectivity (XRR) probe to determine the chemical structure, thickness, and density of our PDTTTPD/CdSe films. We also employed transmission electron microscopy (TEM) and atomic force microscopy (AFM) to examine the relationship between the nano-morphology and the device performance.

Results and discussion

Fig. 1a presents the molecular structure of the D/A polymer PDTTTPD (containing alternating rigid, coplanar, electron-rich DTT units and rigid, electron-deficient TPD units) that we used in the photovoltaic device. The synthesis of the PDTTTPD polymers has been described elsewhere.[42] The presence of the

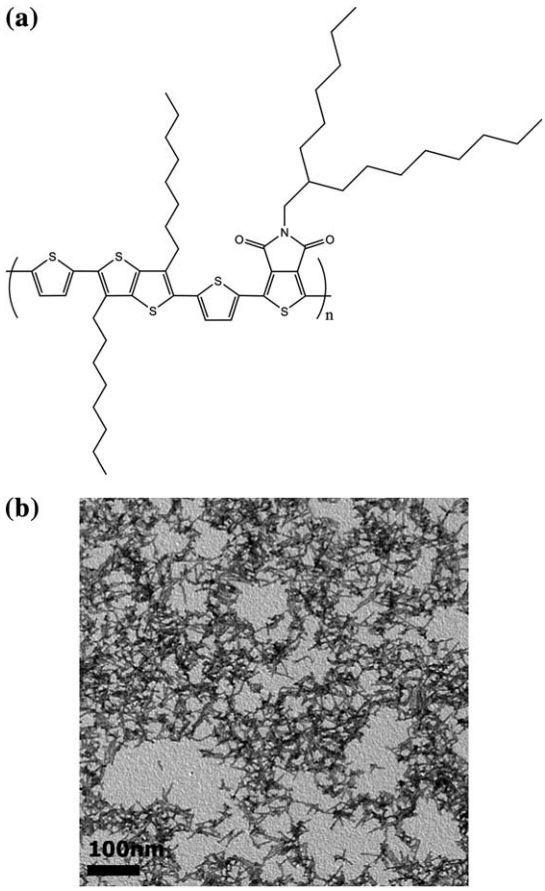

Fig. 1 (a) Molecular structure of PDTTTPD. (b) TEM image of CdSe tetrapods. Scale bar, 100 nm.

DTT and TPD units in the backbone of PDTTTPD provides the copolymer with relatively low-lying HOMO energy levels, resulting in enhanced values of V_{oc} when used in photovoltaic applications. Fig. 1b displays a TEM image of the CdSe tetrapods that we used in the devices. We obtained high yields of these branched nanoparticles; their cores and four arms are clearly evident in the image. The tetrapods' arms had an average diameter of *ca.* 5 nm and lengths in the range 25–50 nm.

Fig. 2a presents the optical absorption spectra of spin-coated films of the pyridine-treated CdSe tetrapods, the pure PDTTTPD, and the PDTTTPD/CdSe (1 : 9, w/w) blend. The thin film of the pyridine-treated CdSe tetrapods exhibits its first absorption peak at 630 nm and a strong absorbance in the shorter wavelength region between 350 and 550 nm, complementing the inferior absorption of the polymers in this region. In the spectrum of the PDTTTPD thin film, we assign the absorption maximum at 510 nm to intramolecular charge transfer between the DTT donor and TPD acceptor. The absorption signal of PDTTTPD was red-shifted by *ca.* 23 nm in thin film relative to that in solution, indicating that considerably strong intermolecular interactions and aggregation occurred in the solid film (see ESI, Fig. S1†). In addition, a vibronic shoulder appeared at 620 nm in the spectrum, attributable to ordered molecular arrangement (*e.g.*, π–π stacking between the polymer backbones) during the precipitation process. The spectrum of the composite film appears as a superposition of the respective

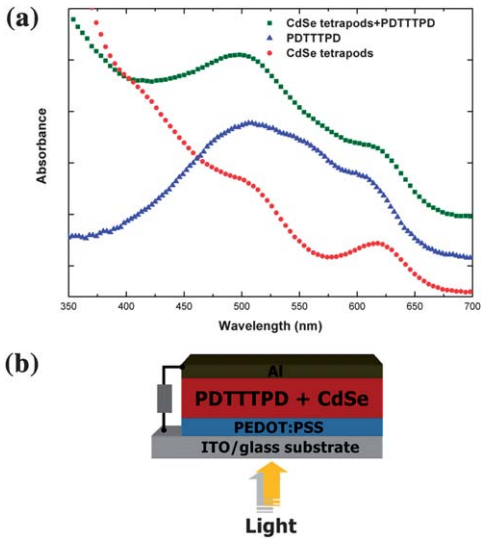

Fig. 2 (a) Optical absorption spectra for spin-coated films of pure PDTTTPD (triangles), pure CdSe tetrapods (circles), and the PDTTTPD/CdSe tetrapod blend (squares). (b) Schematic structure of a PDTTTPD/CdSe tetrapod photovoltaic device.

absorption spectra of the pure PDTTTPD and CdSe components; therefore, no electronic interaction occurred between the PDTTTPD polymer strands and the CdSe tetrapods. Fig. 2b displays the architecture of a fabricated photovoltaic device having the sandwich structure indium tin oxide (ITO)/poly-(3,4-ethylenedioxythiophene):polystyrenesulfonate (PEDOT:PSS)/PDTTTPD:CdSe tetrapods (1 : 9, w/w)/Al. The transparent and conducting ITO layer formed the bottom contact of the device. After coating with PEDOT:PSS, the PDTTTPD/CdSe tetrapod blend was spin-coated from a $CHCl_3$/pyridine/dichlorobenzene solution and then thermally annealed at 130 °C for various lengths of time. Finally, a 100-nm-thick Al film was applied as the top contact, deposited through evaporation directly onto the active layer.

Fig. 3a displays the current density–voltage characteristics of the photovoltaic devices incorporating PDTTTPD/CdSe (1 : 9, w/w) active layers that had been subjected to thermal annealing at 130 °C for 10–30 min. Each device featured a thin PEDOT:PSS hole transport layer to improve the photovoltaic performance and stability;[43] measurements were performed under AM1.5G illumination (100 mW cm^{-2}) in a N_2-filled glove box. The thickness of the active layer in each of these devices was 130 ± 20 nm, as measured using a profilometer. Table 1 lists the short-circuit current densities (J_{sc}), values of V_{oc}, fill factors (FFs), and PCEs of these heterojunction PDTTTPD–CdSe photovoltaic devices. The values of V_{oc} for these blend devices were in the range 0.88–0.89 V, with only slight differences arising from the different annealing times. Because the value of V_{oc} of such a BHJ device is generally associated with the difference between the HOMO energy level of the polymer and the lowest unoccupied molecular orbital (LUMO) energy level of CdSe tetrapods,[44] we suspect that our PDTTTPD/CdSe tetrapod blends exhibited these high values of V_{oc} because of the low-lying HOMO energy level of PDTTTPD. The values of J_{sc} and FF of the PDTTTPD/CdSe blend devices after annealing treatment were significantly higher than those of the as-prepared blend

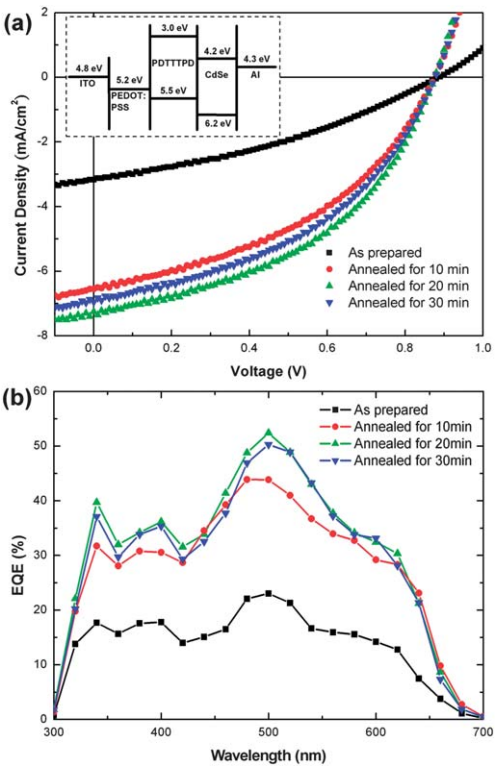

Fig. 3 (a) Current density–voltage characteristics (inset: energy level diagram) and (b) EQE spectra of the PDTTTPD/CdSe tetrapod photovoltaic devices subjected to thermal annealing at 130 °C for various lengths of time. The devices were illuminated under AM1.5G conditions (100 mW cm^{-2}).

device. For example, the value of J_{sc} of the blend device that had been subjected to thermal annealing at 130 °C for 20 min (7.26 mA cm^{-2}) was approximately twice as large as that of the as-prepared blend device (3.16 mA cm^{-2}). Fig. S2† presents the device characteristics of the blends that we had subjected to annealing at temperatures of 110–140 °C. Among them, the device containing the PDTTTPD/CdSe blend that had been thermally treated at 130 °C for 20 min exhibited the highest PCE (2.9%), nearly three times that of the as-prepared device (1.0%). This kind of enhancement also is observed for devices with less CdSe tetrapods such as devices containing PDTTTPD/CdSe tetrapod (1 : 5, w/w) active layer (see Fig. S3†). As a comparison, the photovoltaic study on devices based on P3HT/CdSe tetrapod (1 : 9, w/w) blend system was also carried out (see Fig. S4†), and the results show that the phenomenon is the same for both cases.

Table 1 Photovoltaic parameters of the PDTTTPD/CdSe tetrapod photovoltaic devices prepared with thermal annealing at 130 °C for various lengths of time. Devices were illuminated under AM1.5G conditions (100 mW cm^{-2})

	V_{oc}[a]/V	J_{sc}[b]/mA cm^{-2}	FF[c] (%)	η[d] (%)
As-prepared	0.89	3.16	36	1.0
10 min	0.88	6.56	42	2.4
20 min	0.88	7.26	46	2.9
30 min	0.88	6.95	43	2.6

[a] V_{oc}: open-circuit voltage. [b] J_{sc}: short-circuit current density. [c] FF: fill factor. [d] η: PCE. Solar: AM1.5G (100 mW cm^{-2}).

In addition, the stability study of the device shows that the PCE of the device decreased to 1.5% from 2.9% after the device had been stored in a N_2-filled glove box for 7 days.

The inset to Fig. 3a displays the energy band diagram for the various layers in the device; the energy level offset between the PDTTTPD polymer and the CdSe tetrapods indicates that the tetrapods acted as electron acceptors and the polymer strands as hole acceptors for the dissociation of photogenerated excitons. A previous study[42] determined the HOMO and LUMO energy levels of PDTTTPD to be −5.5 and −3.0 eV, respectively. The presence of the strongly electron-withdrawing TPD moieties provided the polymer with a low-lying HOMO energy level; moreover, the HOMO energy level of PDTTTPD (−5.5 eV) was located significantly below −5.2 eV, suggesting that it has good stability against oxidization in air,[39] a property that we would expect to enhance device stability.

We also measured the external quantum efficiencies (EQEs) of the devices that had been subjected to annealing at 130 °C for various lengths of time. Fig. 3b displays the EQE curves of the devices containing active layers of PDTTTPD/CdSe (1 : 9, w/w); each device exhibited a broad EQE response from 300 to 700 nm. Moreover, the broad peaks observed at wavelengths of less than 450 nm, where PDTTTPD absorbs only slightly, are presumably absorptions due to the CdSe tetrapods. Furthermore, in the range from 320 to 650 nm, the absolute EQEs of the devices incorporating the PDTTTPD/CdSe tetrapod films annealed at 130 °C for different periods of time were much higher than that of the device containing the as-prepared blends. For example, the EQEs at 500 nm for the devices containing the PDTTTPD/CdSe tetrapods that had been annealed at 130 °C for 20 min and the as-prepared film were 53 and 23%, respectively—a two-fold increase for the former over the latter; at 640 nm, the corresponding values were 21 and 7%, respectively—almost a three-fold increase. We obtained calculated values of J_{sc} by integrating the EQEs with an AM1.5G reference spectrum; the calculated values for the devices processed with annealing at 130 °C for 0, 10, 20, and 30 min were 3.0, 6.2, 6.9, and 6.7 mA cm^{-2}, respectively. These values are in reasonable agreement (within ±5% error) with the corresponding values of J_{sc} (3.1, 6.5, 7.2, and 6.9 mA cm^{-2}, respectively) obtained from the J–V measurements. We suspect that the improvement in the values of J_{sc} after annealing resulted from removal of the pyridine ligands from the surfaces of the CdSe tetrapods, thereby allowing more-efficient charge generation and collection. Because morphological changes in active layer thin films can also improve device performance,[13] we probed the chemical structures, densities, thicknesses, and morphologies of the PDTTTPD/CdSe tetrapod films of the as-prepared device and of the optimal device that had been annealed at 130 °C for 20 min.

Fig. 4 presents the ATR-FTIR spectra of the PDTTTPD/CdSe blend films that had experienced annealing treatment and of the as-prepared PDTTTPD/CdSe blend film; these spectra reveal the nature of the chemical species on the surfaces of the blend films. Because all of the samples contained 90 wt% of CdSe tetrapods in their films, the signals were contributed mostly by the surface species on the CdSe tetrapods. The spectrum of the as-prepared blend film features hill-like signals for C–C and C–N stretching vibrations at 1445 and 1600 cm^{-1}, indicating the presence of pyridine ligands bound to the CdSe nanoparticles.[45] The

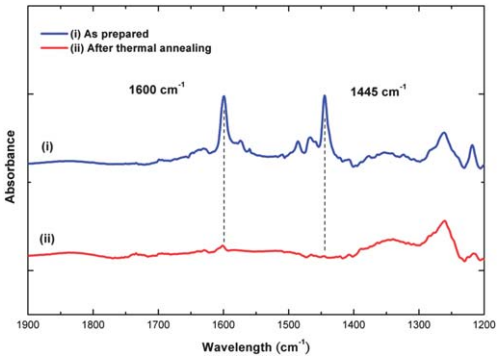

Fig. 4 ATR-FTIR spectra of the PDTTTPD/CdSe tetrapod blend films prepared with and without thermal annealing (130 °C, 20 min).

intensities of both of these signals in the spectra of the annealed films were dramatically reduced relative to those for the as-prepared film, indicating that most of the pyridine ligands on the CdSe tetrapods had been removed, presumably because pyridine is a weakly binding ligand that can be removed thermally.

Fig. 5 presents synchrotron XRR data of the as-prepared and annealed PDTTTPD/CdSe blend films that had been processed through spin-coating of the solutions onto ITO/PEDOT:PSS substrates. Our simulation of the specular reflectivity, allowing us to acquire the physical parameters of the multilayer, was based on the recursive formalism of Parratt;[46] we fitted the reflectivity data with the $Bede_{REFS}$ Mercury code[47] to determine the physical parameters of the multilayer, including its thickness and density. The critical angle of total reflection, as indicated by the dashed line, increased substantially—implying increases in the average film density—after the film had been thermally annealed at 130 °C for 20 min. The fitted densities for the as-prepared and annealed films were 2.9 and 3.2 g cm^{-3}, respectively. Annealing of the PDTTTPD/CdSe tetrapod film caused the thickness of the film to decrease from 150 nm to 135 nm, with an associated increase in the film density. Therefore, removal of pyridine ligands from the CdSe tetrapods decreased the inter-particle distance and, in turn, increased the CdSe tetrapods' packing densities, thereby improving the conductivity in the active layer. We also used grazing incidence X-ray diffraction (GIXRD) to examine the crystallinity of the PDTTTPD polymer strands in films prepared with and without annealing; Fig. S5†

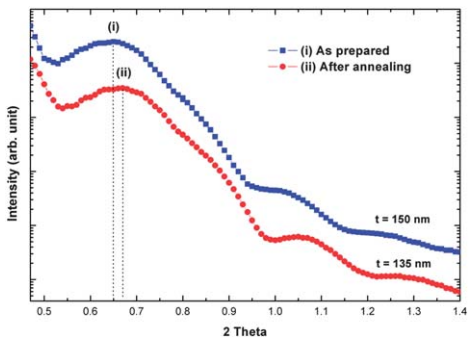

Fig. 5 Synchrotron X-ray reflectance data (log-normal scale) for structures incorporating PDTTTPD/CdSe tetrapod blend layers (on ITO/PEDOT:PSS substrates) prepared with and without thermal annealing (130 °C, 20 min).

reveals, however, that no peaks appeared in either XRD curve. We suspect that the high percentage of three-dimensional CdSe nanostructures (90 wt%) loaded in the blend film destroyed the ordering of the PDTTTPD polymer chains.

Fig. 6 presents TEM images of the blend films used to prepare the devices containing 90 wt% CdSe tetrapods in the films, with and without thermal annealing. The bright and dark regions correspond to PDTTTPD- and CdSe tetrapod-rich domains, respectively, because the electron scattering densities of CdSe (5.6 g cm^{-3}) and polymers (1.1 g cm^{-3}) are quite different. Fig. 6a reveals that the CdSe tetrapods were dispersed rather uniformly in the blended film that had not been subjected to annealing. The degree of aggregation of CdSe tetrapods increased substantially after thermal annealing (Fig. 6b), presumably as a result of the removal of organic ligands from the CdSe surfaces. Furthermore, the PDTTTPD-rich domain in Fig. 6b was larger than that in Fig. 6a; this domain distributed around the CdSe aggregates was clearly evident in the expanded view of the annealed blend film. Consequently, annealing aided in the removal of interfacial pyridine ligands and in bringing the tetrapods closer together. Such aggregation of neighboring tetrapods presumably led to the improved degree of electron transport between tetrapods that occurred after thermal annealing.

Finally, we used AFM (tapping mode) to examine the morphologies of the PDTTTPD/CdSe tetrapod blend films; it is often possible to identify local differences in the composition of a film by comparing its topographic and phase images.[13] The AFM topographic images of the blends (Fig. 7a and b) reveal that annealing led to roughening of the film; the relative surface roughnesses of the films prepared with and without annealing treatment were 9.5 and 6.8 nm, respectively. The roughness of the PDTTTPD/CdSe tetrapod films increases with annealing time (see Fig. S6†), indicating that the aggregation of CdSe tetrapods increases with the annealing time. Such aggregation would, on one hand, improve the electron transport between neighboring tetrapods[13] but, on the other hand, significantly reduce the physical interactions between the tetrapods and the polymer chains, resulting in a reduction of interfacial areas for exciton dissociation since the estimated exciton diffusion length is only ~8 nm in P3HT system.[48,49] Therefore, the devices that have experienced 20 min annealing at 130 °C exhibited the optimal photovoltaic performances (see Fig. S7†). The corresponding AFM phase images (Fig. 7c and d) reveal that the surface roughness was related to the presence of phase domains.

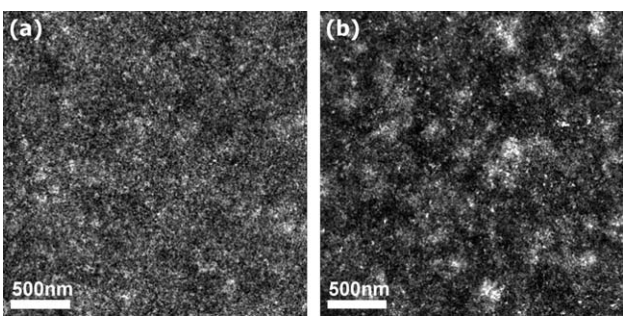

Fig. 6 TEM images of the PDTTTPD/CdSe tetrapod blend films prepared (a) without and (b) with thermal annealing (130 °C, 20 min). Scale bar, 500 nm.

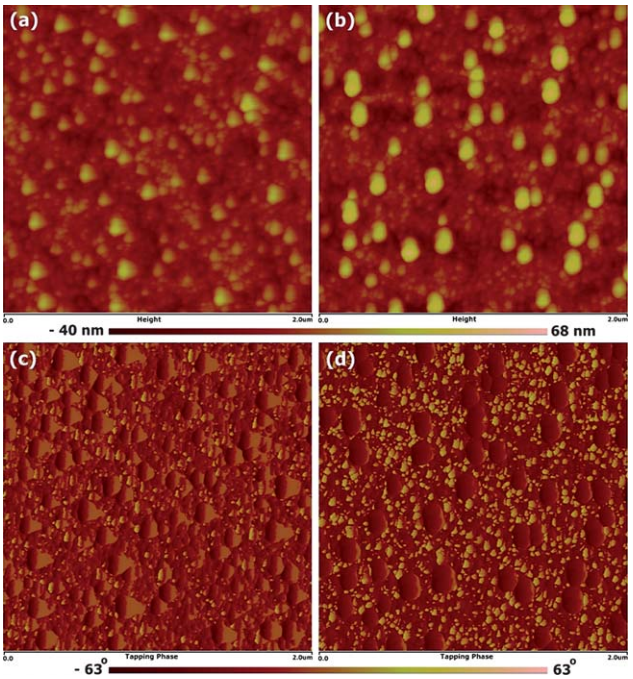

Fig. 7 (a, b) Tapping-mode topographic AFM images and (c, d) corresponding AFM phase images of the (a, c) as-prepared and (b, d) thermally annealed (130 °C, 20 min) PDTTTPD/CdSe tetrapod blend films. Image size, 2 μm × 2 μm.

PDTTTPD polymer grain features are clearly evident in the phase contrast images of the blend films, suggesting that there appears to be little room for the polymer to fully penetrate the tetrapods.[12] Moreover, the minor degree of aggregation of the CdSe tetrapods decreased the space available to the PDTTTPD within the individual tetrapods, resulting in the PDTTTPD polymer grain size in the AFM phase image increasing slightly after thermal annealing. The spin-coating of P3HT/CdSe tetrapod (1 : 9, w/w) blend from chlorobenzene and subsequent thermal annealing result in the phase separation of the two components with a relatively large domain size and give rise to surface-directed spinodal phase separation. The process regime of temporal separation of demixing is attractive because it provides a way to control the morphology and thereby the efficiency of photovoltaic devices.[50]

Conclusions

We have prepared BHJ photovoltaic devices based on PDTTTPD and CdSe tetrapods and optimized their PCE through annealing treatment. In particular, annealing of devices incorporating PDTTTPD/CdSe tetrapod blends (1 : 9, w/w) at 130 °C for 20 min greatly enhanced the AM1.5 PCEs relative to those of the as-prepared blend devices, with an enhancement factor of three. This enhancement resulted from a sharp increase in the short-circuit current density of the device, which contained a more-dense active layer and more highly aggregated CdSe tetrapods after thermal annealing, resulting from the much lower level of pyridine ligands on the CdSe tetrapods. Therefore, the annealing process played an important role in improving the device performance and morphology.

Experimental methods

Materials

PDTTTPD (M_n = *ca.* 9200 g mol^{-1}) was synthesized using a previously reported method[42] and dissolved in 1,2-dichlorobenzene for device fabrication. 1,2-Dichlorobenzene was a better solvent for PDTTTPD than were $CHCl_3$, chlorobenzene, and trichlorobenzene. The CdSe tetrapods were synthesized in a standard Schlenk line according to a previously reported method.[22] Typically, cadmium oxide (0.173 g), octylphosphonic acid (0.535 g), and tri-*n*-octylphosphine oxide (1.293 g) were mixed in a three-neck flask and heated at 300 °C under vigorous stirring and continuous Ar flow for 15 min to obtain a colorless, clear solution. The mixture was cooled to room temperature and then stored in a N_2-filled glove box. After 2 days, this cadmium precursor was heated at 300 °C and then a refrigerated solution of Se (0.213 g) and tributylphosphine (0.635 g) in toluene (0.15 mL) was quickly injected into the hot solution. The temperature of the reaction solution was maintained at 250 °C for the growth of CdSe tetrapods. After performing the reaction for 50 min, the mixture was quenched through the addition of toluene (4 mL). The tetrapods were isolated from the growth mixture through repeated precipitations with MeOH prior to being dispersed in toluene. For ligand exchange, the as-synthesized CdSe tetrapods were redispersed in anhydrous pyridine and stirred continuously at 110 °C overnight in a N_2-filled glove box to remove the original ligands. Finally, the resultant tetrapods were precipitated with anhydrous hexane and redispersed in anhydrous pyridine/$CHCl_3$ (1 : 9) for device fabrication. All other reagents were used as received from commercial sources, without further purification.

Material characterization

ATR-FTIR spectra were recorded at room temperature using a Perkin–Elmer Spectrum100 instrument; optical absorption data were acquired using a Hitachi U-4100 spectrophotometer equipped with an integrating sphere. Synchrotron XRR analyses were performed at the wiggler beamline BL-17B1 using an eight-circle diffractometer at the National Synchrotron Radiation Research Center (NSRRC), Hsinchu, Taiwan; the photon energy was 8 keV and the flux was estimated to be 10^{11} photons s^{-1}. The use of two pairs of slits between the sample and the detector provided a typical wave-vector resolution of *ca.* 0.001 nm^{-1} in the vertical scattering plane. TEM images were obtained using an FEI Tecnai Spirit TWIN instrument operated at 120 keV. The devices were first placed into water; after the active layers had floated to the surface, they were transferred to the TEM grid. The devices' morphologies were recorded under ambient conditions using an atomic force microscope operated in the tapping mode and a Veeco Innova instrument.

Device fabrication and characterization

The current density–voltage (*J–V*) characteristics were investigated for devices having the sandwich structure ITO/PEDOT:PSS/PDTTTPD:CdSe tetrapods (1 : 9, w/w)/Al. The patterned ITO on the glass substrate (5 Ω sq.$^{-1}$, Merck) was cleaned through sequential ultrasonic treatment with detergent, MeOH, acetone, and isopropanol and then dried under a flow of N_2. PEDOT:PSS (Baytron P VP AI 4083) was then spin-coated on the UV ozone-treated ITO and annealed at 150 °C for 1 h before transferring to a N_2-filled glove box. The PDTTTPD/CdSe tetrapod blend solution (28 mg mL^{-1}) was spin-coated (900 rpm, 60 s) on top of the PEDOT:PSS layers. The thickness of the active layers was typically 130 ± 20 nm, as measured using a Veeco Dektak 150 surface profilometer. Subsequently, the active layers of the devices were dried in a covered dish for 1 h and then thermally annealed (130 °C, 20 min) prior to electrode deposition. Using a base pressure of *ca.* 10^{-7} torr, 100 nm Al top electrodes were deposited onto all of the samples by thermal evaporation through a shadow mask. Four devices were fabricated on each substrate, each with an active area of 0.04 cm^2.

The *J–V* characteristics were measured by illuminating the devices through a mask that fitted the electrode crossing area under simulated AM1.5G irradiation (100 mW cm^{-2}) using a Xe lamp-based Newport 66902 150-W solar simulator equipped with a Keithley 2400 source measurement unit. The spectral mismatch factor was calculated by comparing the solar simulator spectrum with the AM1.5G (ASTM G173) spectrum. EQEs were measured using an SR150 (Optosolar GmbH, Germany) spectral response measurement setup.

Acknowledgements

This study was supported financially by the National Science Council of Taiwan (NSC 99-2120-M-009-003) and the US Air Force Office of Scientific Research (AOARD-094039).

References

1 M. Granström, K. Petritsch, A. C. Arias, A. Lux, M. R. Andersson and R. H. Friend, *Nature*, 1998, **395**, 257.
2 C. R. McNeill, J. J. M. Halls, R. Wilson, G. L. Whiting, S. Berkebile, M. G. Ramsey, R. H. Friend and N. C. Greenham, *Adv. Funct. Mater.*, 2008, **18**, 2309.
3 S. C. Veenstra, J. Loos and J. M. Kroon, *Progr. Photovolt.: Res. Appl.*, 2007, **15**, 727.
4 M. M. Koetse, J. Sweelssen, K. T. Hoekerd, H. F. M. Schoo, S. C. Veenstra, J. M. Kroon, X. Yang and J. Loos, *Appl. Phys. Lett.*, 2006, **88**, 083504.
5 H. Y. Chen, J. Hou, S. Zhang, Y. Liang, G. Yang, Y. Yang, L. Yu, Y. Wu and G. Li, *Nat. Photonics*, 2009, **3**, 649.
6 W. Ma, C. Yang and A. J. Heeger, *Adv. Mater.*, 2007, **19**, 1387.
7 B. Kippelen and J. L. Brédas, *Energy Environ. Sci.*, 2009, **2**, 251.
8 S. B. Darling, *Energy Environ. Sci.*, 2009, **2**, 1266.
9 Y. Zhang, S. K. Hau, H. L. Yip, Y. Sun, O. Acton and A. K. Y. Jen, *Chem. Mater.*, 2010, **22**, 2696.
10 T. Ameri, G. Dennler, C. Lungenschmied and C. J. Brabec, *Energy Environ. Sci.*, 2009, **2**, 347.
11 K. M. Noone, E. Strein, N. C. Anderson, P. T. Wu, S. A. Jenekhe and D. S. Ginger, *Nano Lett.*, 2010, **10**, 2635.
12 I. Gur, N. A. Fromer, C. P. Chen, A. G. Kanaras and A. P. Alivisatos, *Nano Lett.*, 2007, **7**, 409.
13 W. U. Huynh, J. J. Dittmer, W. C. Libby, G. L. Whiting and A. P. Alivisatos, *Adv. Funct. Mater.*, 2003, **13**, 73.
14 Y. Zhou, M. Eck and M. Krüeger, *Energy Environ. Sci.*, 2010, **3**, 1851.
15 D. V. Talapin, J. S. Lee, M. V. Kovalenko and E. V. Shevchenko, *Chem. Rev.*, 2010, **110**, 389.
16 S. A. McDonald, G. Konstantatos, S. Zhang, P. W. Cyr, E. J. D. Klem, L. Levina and E. H. Sargent, *Nat. Mater.*, 2005, **4**, 138.
17 D. H. Cui, J. Xu, T. Zhu, G. Paradee, S. Ashok and M. Gerhold, *Appl. Phys. Lett.*, 2006, **88**, 183111.
18 B. Q. Sun and N. C. Greenham, *Phys. Chem. Chem. Phys.*, 2006, **8**, 3557.

19 Y. F. Zhou, F. S. Riehle, Y. Yuan, H. F. Schleiermacher, M. Niggemann, G. A. Urban and M. Krüeger, *Appl. Phys. Lett.*, 2010, **96**, 013304.
20 J. S. Liu, T. Tanaka, K. Sivula, A. P. Alivisatos and J. M. J. Fréchet, *J. Am. Chem. Soc.*, 2004, **126**, 6550.
21 J. D. Olson, G. P. Gray and S. A. Carter, *Sol. Energy Mater. Sol. Cells*, 2009, **93**, 519.
22 B. Q. Sun, E. Marx and N. C. Greenham, *Nano Lett.*, 2003, **3**, 961.
23 B. Q. Sun, H. J. Snaith, A. S. Dhoot, S. Westenhoff and N. C. Greenham, *J. Appl. Phys.*, 2005, **97**, 014914.
24 Y. Zhou, Y. C. Li, H. Z. Zhong, J. H. Hou, Y. Q. Ding, C. H. Yang and Y. F. Li, *Nanotechnology*, 2006, **17**, 4041.
25 P. Wang, A. Abrusci, H. M. P. Wong, M. Svensson, M. R. Andersson and N. C. Greenham, *Nano Lett.*, 2006, **6**, 1789.
26 S. Dayal, N. Kopidakis, D. C. Olson, D. S. Ginley and G. Rumbles, *Nano Lett.*, 2010, **10**, 239.
27 S. Dayal, M. O. Reese, A. J. Ferguson, D. S. Ginley, G. Rumbles and N. Kopidakis, *Adv. Funct. Mater.*, 2010, **20**, 2629.
28 Y. Wu and G. Zhang, *Nano Lett.*, 2010, **10**, 1628.
29 C. Y. Kuo, M. S. Su, C. S. Ku, S. M. Wang, H. Y. Lee and K. H. Wei, *J. Mater. Chem.*, 2011, DOI: 10.1039/c0jm04417b.
30 D. V. Talapin and C. B. Murray, *Science*, 2005, **310**, 86.
31 J. M. Luther, M. Law, Q. Song, C. L. Perkins, M. C. Beard and A. J. Nozik, *ACS Nano*, 2008, **2**, 271.
32 R. Debnath, J. Tang, D. A. Barkhouse, X. Wang, A. G. Pattantyus-Abraham, L. Brzozowski, L. Levina and E. H. Sargent, *J. Am. Chem. Soc.*, 2010, **132**, 5952.
33 B. Kim, B. Ma, V. R. Donuru, H. Liu and J. M. J. Fréchet, *Chem. Commun.*, 2010, **46**, 4148.
34 J. C. Bijleveld, V. S. Gevaert, D. D. Nuzzo, M. Turbiez, S. G. J. Mathijssen, D. M. de Leeuw, M. M. Wienk and R. A. J. Janssen, *Adv. Mater.*, 2010, **22**, E242.
35 Y. T. Chang, S. L. Hsu, M. H. Su and K. H. Wei, *Adv. Mater.*, 2009, **21**, 2093.
36 F. Huang, K. S. Chen, H. L. Yip, S. K. Hau, O. Acton, Y. Zhang, J. Luo and A. K. Y. Jen, *J. Am. Chem. Soc.*, 2009, **131**, 13886.
37 C. Piliego, T. W. Holcombe, J. D. Douglas, C. H. Woo, P. M. Beaujuge and J. M. J. Fréchet, *J. Am. Chem. Soc.*, 2010, **132**, 7595.
38 A. Najari, S. Beaupré, P. Berrouard, Y. Zou, J. R. Pouliot, C. L. P. érusse and M. Leclerc, *Adv. Funct. Mater.*, 2010, **21**, 718.
39 Y. Zou, A. Najari, P. Berrouard, S. Beaupré, B. R. Aïch, Y. Tao and M. Leclerc, *J. Am. Chem. Soc.*, 2010, **132**, 5330.
40 M. C. Yuan, M. Y. Chiu, S. P. Liu, C. M. Chen and K. H. Wei, *Macromolecules*, 2010, **43**, 6936.
41 Y. Kim, S. Cook, S. M. Tuladhar, S. A. Choulis, J. Nelson, J. R. Durrant, D. D. C. Bradley, M. Giles, I. Mcculloch, C. S. Ha and M. Ree, *Nat. Mater.*, 2006, **5**, 197.
42 G. Y. Chen, Y. H. Cheng, Y. J. Chou, M. H. Su, C. M. Chen and K. H. Wei, *Chem. Commun.*, 2011, **47**, 5064.
43 C. Y. Kuo, M. S. Su, Y. C. Hsu, H. N. Lin and K. H. Wei, *Adv. Funct. Mater.*, 2010, **20**, 3555.
44 M. C. Scharber, D. Muhlbacher, M. Koppe, P. Denk, C. Waldauf, A. J. Heeger and C. J. Brabec, *Adv. Mater.*, 2006, **18**, 789.
45 B. S. Kim, L. Avila, L. E. Brus and I. P. Herman, *Appl. Phys. Lett.*, 2000, **76**, 3715.
46 L. G. Parratt, *Phys. Rev.*, 1954, **95**, 359.
47 D. K. Bowen and B. K. Tanner, *Nanotechnology*, 1993, **4**, 175.
48 P. E. Shaw, A. Ruseckas and I. D. W. Samuel, *Adv. Mater.*, 2008, **20**, 3516.
49 M. Y. Chiu, U. S. Jeng, C. H. Su, K. S. Liang and K. H. Wei, *Adv. Mater.*, 2008, **20**, 2573.
50 Y. Vaynzof, D. Kabra, L. Zhao, L. L. Chua, U. Steiner and R. H. Friend, *ACS Nano*, 2011, **5**, 329.

